ADVANCED FUNCTIONAL MATERIALS
www.afm-journal.de

Spontaneous and Directional Transportation of Gas Bubbles on Superhydrophobic Cones

Cunming Yu, Moyuan Cao, Zhichao Dong, Jingming Wang, Kan Li,* and Lei Jiang**

Understanding the behavior of gas bubbles in aqueous media and realizing their spontaneous and directional manipulation are of vital importance in both scientific research and industrial applications, owing to their significant influences on many processes, such as waste water treatment, gas evolution reactions, and the recovery of valuable minerals. However, the behaviors of gas bubbles in aqueous media are mainly dominated by the buoyant force, which greatly impedes gas bubble transportation to any other direction except upward. Consequently, the spontaneous and directional transportation of gas bubbles in aqueous media is still identified as a big issue. Here, superhydrophobic copper cones have been successfully fabricated by integrating low-surface-tension chemical coatings with conical morphology. The generated superhydrophobic copper cones are capable of transporting gas bubbles from their tip to the base spontaneously and directionally underwater, even when they are vertically fixed with tips pointing up. The present study will inspire people to develop novel strategies to achieve efficient manipulation of gas bubbles in practical applications.

1. Introduction

Gas bubbles in aqueous media are ubiquitous in natural world, industrial production, and daily life. Examples include the utilizations of gas bubble in wastewater treatment, recovery of valuable minerals from ores, and pressure sensors.[1] Meanwhile, gas bubbles in liquid transportation systems could cause serious erosions and blockages, further reducing the equipment lifetime as well as wasting resources.[2] Understanding the behaviors of gas bubbles and realizing the reliable bubble manipulation in aqueous media are therefore crucial to both scientific research and industrial applications.[3] Most of the manipulation methods are mainly under the assistance of buoyancy, and gas bubble only moves upward.[3d,4] Furthermore, the buoyancy-driven method has little effect on the microscopic gas bubbles because of their tiny buoyancy.[5] Thus, it is of great importance to realize directional transportation of gas bubbles in aqueous media, especially for microscopic gas bubbles. Previous studies demonstrated that the spontaneous and directional transportation could occur between two bubbles with different volumes on a superhydrophobic porous material.[6] However, the direction and efficiency of bubble transportation depended on the differences between the bubble volumes. It is impossible for a single bubble to be transported downsides. Furthermore, the fabrication of the superhydrophobic porous structures is complex. Therefore, the realization of reliable strategies to spontaneous and directional transporting bubbles is still a timely issue and is urgently needed.

After billions of years of evolution, nature's creatures have evolved intriguing survival skills to provide human beings with enormous inspirations. Spider silks (*Uloborus walckenaerius*) and cactus spines (*Opuntia microdasys*) perform excellent abilities of effectively capturing and directionally transporting tiny water droplets from environment as additional water supply.[7] The cooperation of surface energy, surface gradient, and Laplace pressure is the basis for these outstanding abilities.[8] Inspired by the directional water droplet transportation ability of spider silks and cactus spines, the conical morphology of these biological systems may be capable of spontaneously and directionally transporting gas bubbles underwater.

Herein, a strategy that transcends nature is demonstrated to spontaneously and directionally transport gas bubbles through the employment of superhydrophobic cones. After immersing the superhydrophobic cones in water, a continuous and stable gas film is formed on the cone surface, which contributes to the capture of gas bubbles and the reduction of hysteresis. Subsequently, under the assistance of the Laplace pressure gradient on the conical morphology, the gas bubbles could spontaneously and directionally move toward the base of the cone, even with the cone tip pointing up. After investigating the factors that influenced the bubbles transportation efficiency, we found

Dr. C. Yu, Dr. Z. Dong, Prof. L. Jiang
Beijing National Laboratory for Molecular Sciences (BNLMS)
Key Laboratory of Organic Solids
Institute of Chemistry
Chinese Academy of Sciences
Beijing 100190, China
E-mail: jianglei@iccas.ac.cn
Dr. M. Cao, Dr. J. Wang, Prof. L. Jiang
School of Chemistry and Environment
Beihang University
Beijing 100191, China
E-mail: wangjm@buaa.edu.cn
Dr. K. Li
Laboratory of Bio-inspired Smart Interface Science
Technical Institute of Physics and Chemistry
Chinese Academy of Sciences
Beijing 100190, China
E-mail: likan@iccas.ac.cn

DOI: 10.1002/adfm.201505234

that the bubbles with smaller sizes exhibited higher transportation velocity on cones. In addition, higher apex angles of cones were proved to be a benefit for the bubble transportation. Compared with existing methods of gas bubble manipulation, the proposed approaches realize the spontaneous and directional transportation of single gas bubble by facilely using a superhydrophobic cone. This study will provide an inspiration for people to design new strategies to achieve the spontaneous and directional transportation of gas bubbles and further bloom the researches of gas bubbles in aqueous mediums.

2. Results and Discussion

2.1. Influence of the Wettability of Copper Cones on Gas Bubble Directional Transportation

2.1.1. Fabrication of Copper Cones with Different Wettability

To investigate the relationship between gas bubble transportation and wettability of the cone surfaces, four kinds of copper cones with superhydrophilicity, hydrophilicity, hydrophobicity, and superhydrophobicity are prepared, as shown in **Figure 1**a (see details in the Experimental Section). Figure 1b shows the surface morphology of the superhydrophilic cone, which is composed of microstructured $Cu(OH)_2$ arrays. Since the high surface energy of hydroxides and the microscaled roughness, a low water contact angle (CA) closed to 0° is achieved on the superhydrophilic surface (Figure S1a, Supporting Information).[9] For hydrophilic and hydrophobic cones, similar surface morphologies are shown in Figure 1c,d, which consists of numerous hill-like papillae. However, after chemical modification, different wettability is observed. In detail, an hydrophilic hydroxyl terminal alkanethiol is assembled on the copper cone surface and the CA of which is 38.3° ± 3.4°, whereas another hydrophobic methyl terminal group alkanethiol decorating on copper cone surface results in a CA of 128.8° ± 1.1° (Figure S1b,c, Supporting Information).[10] The surface of superhydrophobic cone is composed of numerous microhill-like papillae and hydrophobic nanosilica particles (Figure 1e), which facilitate the surface with a high CA of 156.2° ± 3.0° (Figure S1d, Supporting Information).[11]

2.1.2. The Behaviors of Gas Bubbles on Copper Cones with Different Wettability

To minimize the effect of buoyancy and reveal the influence of surface wettability on the behaviors of gas bubbles on cone surfaces, the cones with different wettabilities are horizontally placed underwater (**Figure 2**; Figure S2, Supporting Information). Figure 2a,b illustrates that the superhydrophilic and hydrophilic cones fail to trap or transport gas bubbles. When the gas bubble impact with the superhydrophilic or hydrophilic cone, it could bounce off. In contrast, the hydrophobic one has bubble transportation ability partially, where gas bubbles can be trapped and transported for a short distance. This transportation process could only be accomplished through the continuous coalescence of gas bubbles that finally escape into water owing to the enlarged buoyancy (Figure 2c). As shown in Figure 2d, the superhydrophobic cones can trap gas bubbles efficiently and transport the captured bubbles to their base in a high velocity. Moreover, the bubbles can be singly transported to the base of superhydrophobic cones without the assistance of bubbles coalescence.

2.2. Influence of Bubble Volume and Cone Apex Angle on the Bubbles Transportation Processes

The volumes of gas bubbles and the apex angles of cones are both crucial to the gas bubble transportation process. The

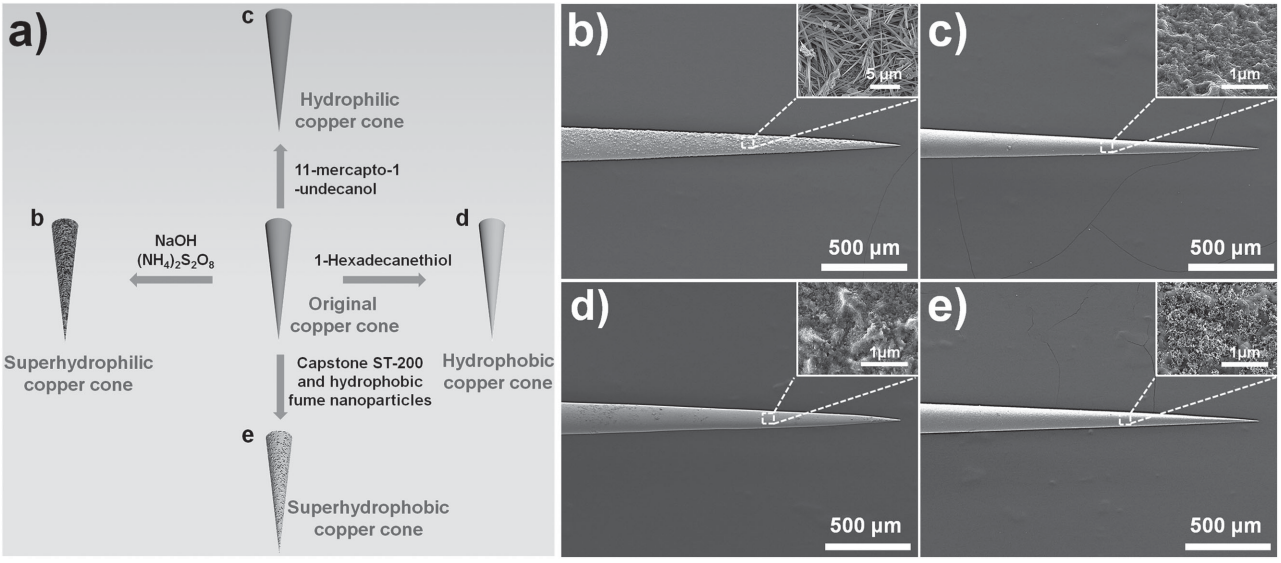

Figure 1. Fabrication process and SEM images of copper cones with various wettabilities. a) Fabrication process of copper cones. b) The superhydrophilic copper cone with numerous $Cu(OH)_2$ arrays. c,d) The hydrophilic and hydrophobic cones with similar surface microstructures, i.e., numerous hill-like papillae. e) The superhydrophobic cone with microhill-like papillae and nanosilica particles.

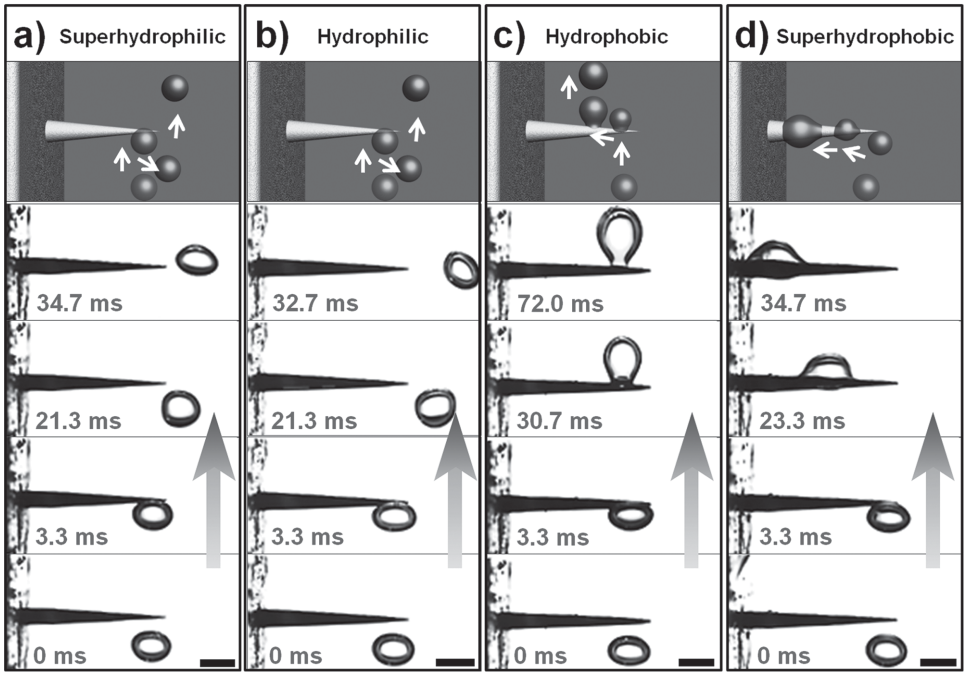

Figure 2. In situ observation of the bubbles transportation process on copper cones with different wettabilities. a,b) The gas bubbles squashed and then bounced off when contacting with the superhydrophilic and hydrophilic cones. c) The gas bubble was captured and transported for a short distance under the assistance of coalescence on the hydrophobic cones. Finally, the coalesced bubble escaped into water before reaching the base of cones. d) The gas bubble was spontaneously and directionally transported to the base of superhydrophobic cones. Scale bars, a–d): 2 mm.

morphological characteristics of gas bubbles with different volumes on the same superhydrophobic cone are different. As shown in **Figure 3**a–d, small gas bubbles present the barrel shape on superhydrophobic cone with the apex angle of 5°, while the large ones present the hemisphere shape. The transportation distances (L) of gas bubbles with different volumes with variation of time (t) on the cone with apex angle of 5° are illustrated in Figure 3e. L is increased with the increase of t. After linearly fitting, the relationship between L and t is approximately linear, as indicated by the solid line. That is to say, the whole transportation process of gas bubbles can be approximately regarded as uniform motion state. The experimental average velocities of 0.02, 0.50, 4.20, and 14.20 µL gas bubbles on apex angle 5° cones are 69.8 ± 1.2, 40.7 ± 2.1, 30.9 ± 0.9, and 25.8 ± 0.2 cm s^{-1}, respectively. They are very close to the gas bubble velocities obtained from the linear fitting functions (71.3 cm s^{-1} of 0.02 µL, 36.7 cms^{-1} of 0.50 µL, 29.0 cm s^{-1} of 4.20 µL, and 22.9 cm s^{-1} of 14.2 µL). The transportation velocities on superhydrophobic cones can be approximately considered as the average velocities of gas bubbles. Moreover, Figure 3e demonstrates that the transportation velocities of gas bubbles are increased with the decrease of the volumes of gas bubbles. The transportation efficiencies of superhydrophobic cones are much higher for bubbles with miniature sizes. In addition, the apex angles of superhydrophobic cones play an important role in determining the bubbles transportation properties. As shown in Figure 3f and Figure S3 (Supporting Information), with the increasing of apex angles, the transportation velocities of bubbles on superhydrophobic cones are significantly increased, especially for tiny bubbles with a volume of 0.02 µL. The transportation velocities are 0 cm s^{-1} at 0°, 34.6 ± 1.7 cm s^{-1} at 3°, 69.8 ± 1.2 cm s^{-1} at 5°, 72.6 ± 6.3 cm s^{-1} at 7°, and 79.8 ± 4.8 cm s^{-1} at 9°, respectively. It can be concluded that both the miniature size of bubble and the high apex angle of cone endow the gas bubbles with distinguished spontaneous and directional transporting performance on the superhydrophobic cones.

2.3. Bubbles Transportation on Superhydrophobic Copper Cones with Various Tilt Angles

Bubbles transportation on superhydrophobic cones that are placed at varied tilt angles (90°, 45°, −45°, and −90°) are investigated (**Figure 4**). When the cone is fixed with the tip pointing down, the gas bubbles are able to rapidly move to the base of the superhydrophobic cones with velocity of ≈41.1 cm s^{-1} (Figure 4a). Inclining the tilt angle of cones to 45°, as shown in Figure 4b, the transportation velocity of bubble is correspondingly decreased to ≈32.1 cm s^{-1}. If the tilt angles of cones are below 0°, the gas bubbles still transport along the cones (Figure 4c,d). However, the gas bubbles will cease their movements before reaching the base side of superhydrophobic cones. The transportation distance of bubbles on cones with a tilt angle of −45° is larger than that on cones with a tilt angle of −90°. To better demonstrate that the transportation process is spontaneous and directional, we have prepared wave-shaped superhydrophobic cone with a length of ≈2 cm, on particular sections of which the buoyant force is the resistant force impeding the movement of gas bubbles. However, under the assistance of Laplace pressure, the bubbles could overcome the resistance of buoyancy and rapidly move toward the base side of cones with a velocity of ≈29.9 cm s^{-1} (Figure 4e).

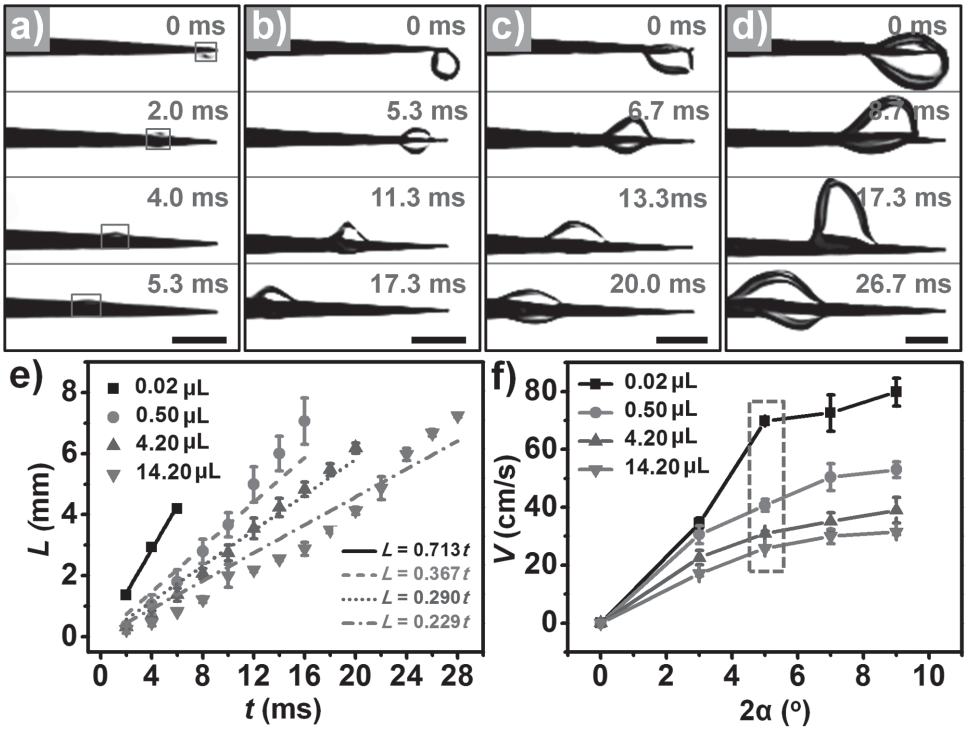

Figure 3. a–d) In situ observation of the spontaneous and directional gas bubbles transportation processes on the superhydrophobic cone with the apex angle of 5°. The gas bubbles vary with the following volumes: 0.02, 0.50, 4.20, and 14.20 μL, respectively. e) The linear fit of transportation distance (L) with respect to the transportation time (t) of gas bubbles with different volumes (0.02, 0.50, 4.20, and 14.20 μL) on cone with apex angle of 5°. The linear fitting line is close to the experimental results. L can be approximately predicted by using the linear functions. f) Variation of transportation velocities of gas bubble with different volumes with respect to angle apexes of superhydrophobic copper cones. Scale bars, a–d): 2.0 mm.

2.4. The Underlying Mechanism for the Factors (Wettability, Volume, Apex Angle, and Tilt Angle) Influencing the Bubble Transportation Behaviors on Copper Cones

By investigating the behaviors of bubbles on the as-prepared cones, we have found that the transportation abilities of cones are mainly determined by two factors. One is being capable of efficiently trapping gas bubbles and the other is being able to provide sufficient driven force acting on gas bubbles. The former is determined by the wettability of copper cone. The latter mainly depends on the axis-direction component of the resultant force (F) on the bubbles.

2.4.1. The Mechanism for Wettability Influencing the Behaviors of Gas Bubbles

After immersing the superhydrophilic and hydrophilic cones in water, their surfaces could easily absorb water films. This water entrapment greatly hinders the gas bubbles from contacting with the solid surfaces.[12] Consequently, the underwater bubble contact angles on the superhydrophilic and hydrophilic surfaces are 154.8° ± 2.0° and 154.6° ± 1.2°, respectively (Figure S4a,b, Supporting Information). Low gas adhesive forces with values closed to 0 μN are observed on both of these two surfaces (Figure S5a,b, Supporting Information). In contrast, the hydrophobic surfaces show low affinities to water with a small bubble contact angle of 108.3° ± 3.1° (Figure S4c, Supporting Information) and a large bubble adhesive force of 167.0 ± 14.0 μN (Figure S5c, Supporting Information), which are originated from the intrinsically low surface energy of chemical composition and the decoration of micro/nano bubbles.[13] Consequently, the gas bubbles can easily replace the unstable water entrapment and pins to the hydrophobic surface (i.e., hydrophobic interaction). The superhydrophobic surfaces demonstrate superaerophilic property underwater with a small bubble contact angle of nearly 0° (Figure S4d, Supporting Information) and a high bubble adhesive force of 151.3 ± 2.9 μN (Figure S5d, Supporting Information), resulting from the formation of gas film entrapment on the superhydrophobic surface.[14] As the gas bubbles contacts with the superhydrophobic cone, it will be rapidly captured by superhydrophobic cone and subsequently coalesce with the gas film.

2.4.2. The Mechanism for Forces Influencing the Behaviors of Gas Bubbles on Hydrophobic and Superhydrophobic Copper Cones

Figure 5 illustrated the forces acting on the gas bubbles, including the Laplace pressure (F_L), the hysteresis resistance force (F_H), the drag force of water (F_D), and the buoyant force of bubbles ($F_B \sin \beta$, β is the tilt angle between the axis of cone and horizontal line). The resultant force (F) acting on gas bubbles can be deduced as follows

$$F = F_L + F_H + F_D + F_B \sin \beta \quad (1)$$

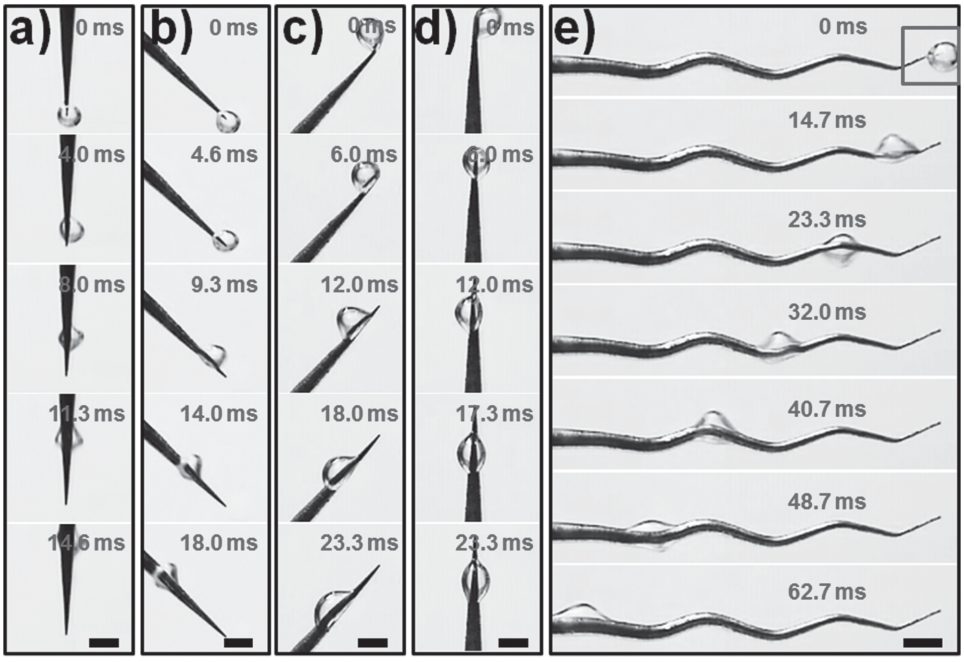

Figure 4. In situ optical observations of the directional bubble transportation on superhydrophobic cones at various tilt angles. a–d) The superhydrophobic cones are placed at various tilt angles, including 90°, 45°, –45°, and –90°, respectively. For cones with the tips pointing up, where the buoyancy is the resistant force, the gas bubbles are also driven toward their base until F_L is equal to F_B. e) The horizontally placed wave-shaped superhydrophobic cones are capable of spontaneously and directionally transporting gas bubbles. F_B is the resistant force on particular sections (red box). Scale bars, a–e): 2.0 mm.

F_L is the axis-direction component of Laplace pressure driving the bubbles spontaneously and directionally toward the base side of cone, which can be described as follows[8a,b]

$$F_L \approx 2\gamma\left(\frac{1}{R_1}-\frac{1}{R_2}\right)S\sin\alpha \tag{2}$$

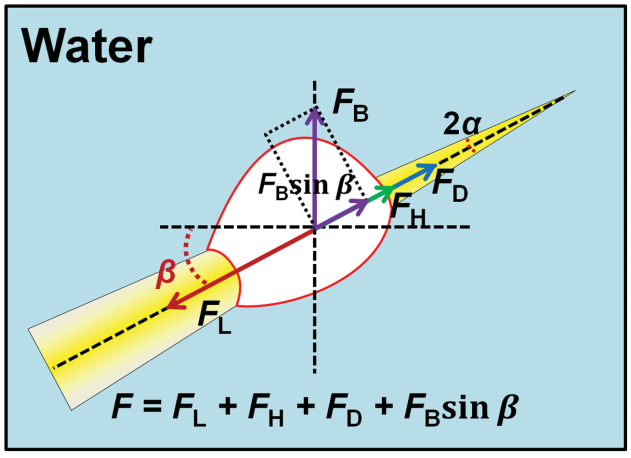

Figure 5. Schematic images of forces acting on a gas bubble. For bubbles transporting on cone placed with certain tilt angle (β), there are mainly four forces influencing its behaviors. They are the axis-direction components of Laplace force (F_L), the hysteresis resistance force (F_H), the drag force of water (F_D), and the buoyancy (F_B sin β). If the tip of the cone points up, β is below 0°. If the cone tip points down, β is above 0°. For the horizontally placed cones, β is equal to 0°. α is the semi-apex angle of the cone.

where γ is the surface tension of water, R_1 and R_2 are the local radius on the two opposite sides of the bubbles, S is the area of the region enclosed by the gas bubble, and α is the semi-apex angle of cones. F_H is the axis-direction component of hysteresis resistance force impeding the movement of bubbles, which can be deduced as follows[15]

$$F_H \approx \pi R_0 \gamma(\cos\theta_r - \cos\theta_a)\cos\alpha \tag{3}$$

where R_0 is the radius of the bubble, and θ_r and θ_a are the receding and advancing contact angles, respectively. F_D is the drag force of water to hinder the movement of gas bubbles, which can be expressed as follows

$$F_D = \frac{1}{2}C_D\rho v^2 A \tag{4}$$

where C_D is the drag coefficient of water, ρ is the density of water, v is the transportation velocity of gas bubbles, A is the cross-sectional area of gas bubbles. The axis-direction component of buoyant force (F_B sin β) is calculated

$$F_B \sin\beta = \rho g V \sin\beta \tag{5}$$

where ρ is the density of water, g is the acceleration of gravity, V is the volume of bubbles, and β is the tilt angle of cones ($-90° < \beta < 90°$).

On the horizontally placed hydrophobic and superhydrophobic cones, their tilt angle (β) is zero. The axis-direction component of buoyant force of bubble (F_B sin β) is nearly equal to zero, which is not large enough to introduce into the bubble

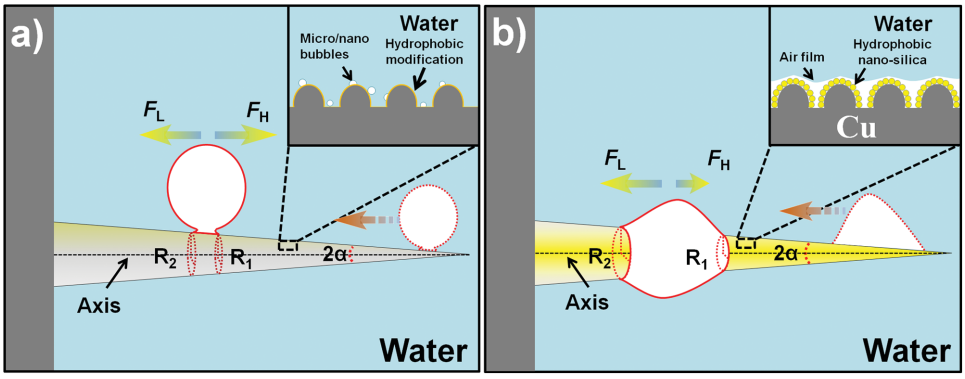

Figure 6. Mechanism of bubble transportation processes on horizontally placed hydrophobic and superhydrophobic cones. a) The surface of hydrophobic cone is decorated by randomly distributed micro/nanoscaled gas bubbles, which could not develop into a continuous gas film and results in a large F_H. b) The surface of superhydrophobic cone is composed of numerous superhydrophobic micro/nano structures, which contribute to the formation of the continuous gas film. Benefiting from the assistance of gas film, the F_H on superhydrophobic cone is very low (nearly 0 μN).

transportation. As shown in **Figure 6**a, on hydrophobic cone, micro/nanoscaled gas bubbles can be trapped on its surface but cannot form a continuous gas film, on which the bubble wetting state/contact mode is considered as three-phase contact and the gas bubbles present a hemisphere shape. Furthermore, as shown in Figure S6a (Supporting Information), the θ_r and θ_a on hydrophobic surface are 88.7° ± 3.1° and 107.2° ± 2.1°, respectively, which illustrates that F_H on hydrophobic surface is above zero according to Equation (3). In contrast, on superhydrophobic cone, a continuous gas film (plastron) can be trapped on its micro/nanostructured surface, which changes the bubble wetting state/contact mode into two-phase contact and enable the gas bubbles present a barrel shape (Figure 6b). Compared with the hemisphere shape, the barrel morphology facilitates the gas bubbles with a bigger enclosed area S and a larger difference of R_1 and R_2. Consequently, F_L acting on superhydrophobic copper cone is larger than that on hydrophobic one. Moreover, both θ_r and θ_a on the superhydrophobic surface are approximate to 0 (Figure S6b, Supporting Information). F_H on superhydrophobic surface is approaching zero. As a consequence, the superhydrophobic cone demonstrates better gas bubbles transportation ability than the hydrophobic one.

2.4.3. The Mechanism for the Volumes of Bubbles and the Apex Angles of Cones Influencing the Bubbles Behaviors on Superhydrophobic Copper Cones

When an object moves in aqueous media, there will be a resistant force generated by the liquid impeding. The Weber number (*We*) is regarded as a measure of relative importance of fluid's inertia to its surface tension.[16] In our experiments, we find that *We* is much less than 1. It indicates that the driven force F_L caused by the surface tension is the dominating factor in controlling gas bubble transportation (see Figure S7 in the Supporting Information for detail). Reynolds number (*Re*) is above 100 in our investigations. It shows that the viscosity resistance of water takes little effect on bubbles transportation (see S8 in the Supporting Information for detail). In addition, in the case of bubbles transportation on horizontally placed superhydrophobic cones, the influence of F_B and F_H could be both ignored. At the moment of bubbles contacting with the superhydrophobic cone, their movement states could be regarded as quasi-static. Thus, drag force of water is neglected. As a result, F is equal to F_L. The initial accelerated speed of gas bubbles (a) is determined by the F_L and their mass (m), which can be deduced as follows

$$a = \frac{F_L}{m} \approx \frac{\gamma}{m}\left(\frac{1}{R_1} - \frac{1}{R_2}\right) S \sin\alpha \tag{6}$$

With the increasing of V, the S on superhydrophobic cone is not significantly increased except for the conformation of gas bubbles changing from barrel to hemisphere shape. It illustrates that the driven forces F_L on these four cases are similar (Figure 3a–d; Figure S9, Supporting Information). However, with the increasing of volume, the mass of relative gas bubble is significantly increased. According to Equation (6), the bubbles with smaller volume are facilitated with larger accelerated speed and consequently they achieve larger velocities over the same time period. The apex angle of superhydrophobic cone is another important factor in determining the efficiency of gas bubble transportation. Larger α ($\alpha \leq 45°$) is beneficial for the enhancement of transportation velocity according to Equation (6).

After achieving uniform movement state, the drag force of water needs to be considered. According to Equations (2) and (3), the velocities of gas bubbles can be approximately deduced as follows (see Figure S10, Supporting Information for detail)

$$v = \sqrt{\frac{24\gamma \tan\alpha}{\rho R}} \tag{7}$$

where γ is the surface tension of water, ρ is the density of water, R is the radius of gas bubble. According to Equation (7), we can obtain the theoretical transportation velocities, which is very close to the experimental values in most cases (Figure S11, Supporting Information).

According to the above proposed mechanism (Equations (2)–(4) and Equation (7)), the bubble can be transported on the whole length of the superhydrophobic cone. In fact, in order to keep the uniform movement state, the

morphological characteristic of a gas bubble on the same superhydrophobic cone kept changing. F_L kept matching with F_D. Thus, the gas bubbles, especially tiny bubbles, might spread completely before arriving to the base side of the cone. However, the gas transportation process did not terminate but continued in another form. The redistribution of the gas film (including the spread gas bubble and the original air layer) made the gas keep transporting to the base side of the cones. The redistribution of the gas film is very complex and not considered in the calculation of theoretical transportation velocities.

2.4.4. The Force Analysis of Bubbles Transporting on Superhydrophobic Cones with Various Tilt Angles

If the tilt angle of cones is not equal to zero, their axis-direction components of buoyant force are not zero. The influence of buoyant force has to be considered. As shown in Figure 4a and Figure S12a (Supporting Information), when the cone is vertically fixed with the tip pointing upside down, the direction of buoyant force is completely same as that of F_L. It facilitates bubbles to achieve the maximum axis-direction component of buoyant force (F_B). As a result, the gas bubbles are endowed with the maximum transportation velocity. With the inclining of the tilt angle (β), the axis-direction component of buoyant force is correspondingly reduced, resulting in the decrease of the transportation velocity of bubbles (Figure 4b; Figure S12b, Supporting Information). When the tilt angle of cone (β) is below 0°, the direction of F_B is opposite to that of F_L. That is to say, the buoyant force is changed to the resistant force. With the decreasing of tilt angles, as shown in Figure S12c,d (Supporting Information), the axis-direction components of buoyant force are becoming larger. If the tilt angle is reaching –90°, the direction of buoyancy is completely opposite to that of F_L. It hinders the movement of gas bubbles with the maximum resistant force ($-F_B$). Therefore, the transportation distance on cones with tilt angle of –90° is the smallest. Astonishingly, the gas bubbles could spontaneously and directionally transport toward the base of the cone by overcoming the resistant force, and continue their movement until F_L is equal to the axis-direction component of buoyant force ($F_B \sin \beta$).

3. Conclusion

In this paper, the superhydrophobic copper cones are successfully fabricated by facilely integrating the low surface chemical coating with conical morphology. The superhydrophobic copper cones exhibit the capability of spontaneously and directionally transporting gas bubbles with various volumes in the aqueous media, especially for microscopic gas bubbles. The behaviors of gas bubbles on copper cones are much influenced by the continuous and stable gas film. Taking advantages of the gas film, the gas bubbles can be efficiently captured and transported on the surfaces of the superhydrophobic cones with very low resistant force. Moreover, the conical morphology is crucial to the transportation processes of gas bubbles. It initiates a gradient of Laplace pressure to drive the directional movement of gas bubbles. Both the miniature size of bubble and the high apex angle of cone are a benefit for the spontaneous and directional transportation of gas bubbles. In addition, the gas bubbles even could overcome the resistance of buoyant force and transport toward the base of the superhydrophobic cones when they are vertically fixed with tips pointing up. We believe that the present work could lead to the further understanding of underwater interface phenomena and provide a new avenue to develop novel strategies to achieve efficient manipulation of gas bubbles in practical applications.

4. Experimental Section

Fabrication and Experiments on Single Copper Cone: Copper cones were fabricated via electro-etching from Copper wires with diameter of 1.0 mm.[8b] After being corroded in the mixed erosion solutions of sodium hydroxide (2.7 M, Beijing Chemical Works) and ammonium persulfate (0.3 M, Beijing Chemical Works) for 30 min, then rinsed with ample deionized water and dried with nitrogen, the superhydrophilic cones were achieved.[9a] The hydrophilic and hydrophobic copper cones were prepared by modifying the original copper cones with 1-dodecanethiol (10.0×10^{-3} M, Sigma-Aldrich) and 11-mercapto-1-undecanol (10.0×10^{-3} M, Sigma-Aldrich) for 24 h, respectively.[10] The superhydrophobic copper cones were prepared by dipping the original copper cones into the acetone solution with the mixture of hydrophobic fume nanoparticles (Aerosil R202, average particle size 14 nm, Evonik Degussa Co.) and Capstone ST-200 (DuPont Co.) for several times. The mixed solution consists of 1.0 g hydrophobic fume nanoparticles, 3 mL Capstone ST-200 and 17 mL acetone. After that, the coated copper cones were heated on a hot plate at 120 °C (Thermo Scientific Co.) for 30 min and then heated at 80 °C in an oven for 1 h.[11]

Methods for Determining the Bubbles Transportation Velocity: The bubbles transportation velocities were achieved from the transportation distance of bubble on horizontally placed superhydrophobic cones and transportation time. Several representative frames were taken from the high-speed video. The moment that gas bubbles contacted with the tip of cones was defined as the starting point of the transportation time (0 ms). The moment that gas bubbles arrived at the base of cones was defined as the ending point (t ms). The transportation distance (L) of bubble was defined as the distance between the front edge of bubbles on starting point and ending point. Then the average velocity (v) can be calculated as follows

$$v = \frac{L}{t}$$

Characterization of the Copper Cones: SEM (scanning electron microscope) images of the samples were obtained with a field-emission scanning electron microscope (S-4800, Japan). The behaviors of the air bubbles on cones were recorded by using a high-speed camera (*i*-SPEED 3, OLYMPUS, Japan). The water and bubble contact angles were measured using a video-based contact angle measuring device (OCA 20, Data-physics, Germany). The interaction force between the gas bubbles and copper surfaces with different wettabilities can be accessed by a high-sensitivity microelectromechanical balance system (DCAT 11, Data-physics, Germany).

Supporting Information

Supporting Information is available from the Wiley Online Library or from the author.

Acknowledgements

This work was supported by the National Research Fund for Fundamental Key Projects (2013CB933000), National Natural Science

Foundation (21421061, 21431009), Beijing National Science Foundation (2152018), Beijing Higher Education Young Elite Teacher Project, the Key Research Program of the Chinese Academy of Sciences (KJZD-EW-M01, KJZD-EW-M03), and the 111 project (B14009). The authors truly thank Prof. David Quéré and Dr. Bin Su for their helpful suggestions.

Received: December 6, 2015
Revised: February 10, 2016
Published online: March 30, 2016

[1] a) H. Odegaard, *Water. Sci. Technol.* **2001**, *43*, 75; b) Md. S. K. A. Sarkar, S. W. Donne, G. M. Evans, *Adv. Powder Technol.* **2010**, *21*, 412; c) D. W. Fuerstenau, R. Herrera-Urbina, *Surfactant Sci. Ser.* **1989**, *33*, 259; d) M. J. F. Warnier, M. H. J. de Croon, E. V. Rebrov, J. C. Schouten, *Microfluid. Nanofluid.* **2010**, *8*, 33.

[2] a) C. A. Fairfield, *Wear* **2014**, *317*, 92; b) A. Philipp, W. Lauterborn, *J. Fluid Mech.* **1998**, *361*, 75; c) S. Fontanesi, M. Giacopini, G. Cicalese, S. Sissa, S. Fantoni, *Eng. Failure Anal.* **2014**, *44*, 408; d) C. Reynolds, M. Yitayew, *Agric. Water Manage.* **1995**, *29*, 25.

[3] a) S. H. Li, R. Furberg, M. S. Toprak, B. Plam, M. Muhammed, *Adv. Funct. Mater.* **2008**, *18*, 2215; b) H. J. Cho, J. P. Mizerak, E. N. Wang, *Nat. Commun.* **2015**, *6*, 8599; c) J. Dokovic, C. W. Tobias, *J. Electrochem. Soc.* **1987**, *134*, 331; d) Y. J. Li, H. C. Zhang, T. H. Xu, Z. Y. Lu, X. H. Wu, P. B. Wan, X. M. Sun, L. Jiang, *Adv. Funct. Mater.* **2015**, *25*, 1737; e) P. T. L. Koh, M. Manickam, M. P. Shwarz, *Miner. Eng.* **2000**, *13*, 1455.

[4] a) R. W. Day, S. W. Dunavent, E. Rich, United States Patent 4326863, **1982**; b) L. E. Lema, United States Patent 5202026, **1993**; c) J. T. Fuss, *Prog. Fish-Cult.* **1986**, *48*, 215.

[5] a) L. Parkinson, R. Sedev, D. Fornasiero, J. Ralston, *J. Colloid Interface Sci.* **2008**, *322*, 168; b) F. Y. Ushikubo, T. Furukawa, R. Nakagawa, M. Enari, Y. Makino, Y. Kawagoe, T. Shiina, S. Oshita, *Colloids Surf. A-Physicochem. Eng. Asp.* **2010**, *361*, 31.

[6] a) F. M. Chang, Y. J. Sheng, S. L. Cheng, H. K. Tsao, *Appl. Phys. Lett.* **2008**, *26*, 264102; b) R. Ma, J. M. Wang, Z. J. Yang, M. Liu, J. J. Zhang, L. Jiang, *Adv. Mater.* **2015**, *14*, 2384; c) J. Chen, Y. Liu, D. Guo, M. Cao, L. Jiang, *Chem. Commun.* **2015**, *51*, 11872.

[7] a) Y. Zheng, H. Bai, Z. Huang, X. Tian, F. Q. Nie, Y. Zhao, J. Zhai, L. Jiang, *Nature* **2010**, *463*, 640; b) J. Ju, H. Bai, Y. Zheng, T. Zhao, R. Fang, L. Jiang, *Nat. Commun.* **2012**, *3*, 1247.

[8] a) É. Lorenceau, D. Quéré, *J. Fluid. Mech.* **2004**, *510*, 29; b) J. Ju, K. Xiao, X. Yao, H. Bai, L. Jiang, *Adv. Mater.* **2013**, *25*, 5937; c) M. Y. Cao, J. Ju, K. Li, S. X. Dou, K. S. Liu, L. Jiang, *Adv. Funct. Mater.* **2014**, *24*, 3235; d) J. Ju, X. Yao, S. Yang, L. Wang, R. Z. Sun, Y. X. He, L. Jiang, *Adv. Funct. Mater.* **2014**, *24*, 6933.

[9] a) W. X. Zhang, X. G. Wen, S. H. Yang, Y. Berta, Z. L. Wang, *Adv. Mater.* **2003**, *15*, 822; b) F. Xia, L. Feng, S. T. Wang, T. L. Sun, W. L. Song, W. H. Jiang, L. Jiang, *Adv. Mater.* **2006**, *25*, 432.

[10] P. Laibinis, G. M. Whitesides, A. N. Parikh, T. Y. Tao, D. L. Allara, R. G. Nuzzo, *J. Am. Chem. Soc.* **1991**, *113*, 7152.

[11] Z. Dong, J. Ma, L. Jiang, *ACS Nano* **2013**, *11*, 10371.

[12] a) C. Shi, X. Cui, L. Xie, Q. Liu, D. Y. C. Chan, J. N. Israelachvili, H. Zeng, *ACS Nano* **2014**, *1*, 95; b) R. F. Tabor, R. Manica, D. Y. C. Chan, F. Grieser, R. R. Dagastine, *Phys. Rev. Lett.* **2011**, *106*, 064501.

[13] a) C. Shi, D. Y. C. Chan, Q. Liu, H. Zeng, *J. Phys. Chem. C* **2014**, *118*, 25000; b) N. Ishida, M. Sakamoto, M. Miyahara, K. Higashitani, *Langmuir* **2000**, *16*, 5681; c) N. Ishida, T. Inoue, M. Miyahara, K. Higashitani, *Langmuir* **2000**, *16*, 6377.

[14] a) J. Wang, Y. Zheng, F. Nie, J. Zhai, L. Jiang, *Langmuir* **2009**, *25*, 14129; b) W. Barthlott, T. Schimmel, S. Wiersch, K. Koch, M. Brede, M. Barczewski, S. Walheim, A. Weis, A. Kaltenmaier, A. Leder, H. F. Bohn, *Adv. Mater.* **2010**, *22*, 2325; c) T. Lauridsen, K. Glavina, T. D. Colmer, A. Winkel, S. Irvine, K. Lefmann, R. Feidenhans'l, O. Pedersen, *J. Struct. Biol.* **2014**, *188*, 61.

[15] K. Li, J. Ju, Z. Xue, J. Ma, L. Feng, S. Gao, L. Jiang, *Nat. Commun.* **2013**, *4*, 2276.

[16] a) A. Frohn, N. Roth, *Dynamics of Droplets*, Springer Science & Business Media, Berlin Heidberg, Germany **2000**; b) P. Day, A. Manz, Y. Zhang, *Microdroplet Technology: Principles and Emerging Applications in Biology and Chemistry*, Springer Science & Business Media, Berlin Heidberg, Germany **2012**.